Nonlinear Viscoelastic Analysis of Thick Walled Cylindrical Composite Pipes

R.M. Guedes

INEGI - Mecânica Experimental e Novos Materiais, Faculdade de Engenharia, Universidade do Porto, Rua Dr. Roberto Frias s/n, 4200-465 Porto, Portugal

ABSTRACT

This paper analyzes the effect of the polymer matrix non-viscoelastic behaviour in the mechanical behaviour of thick multilayered cylinders. The original contribution of this work is to provide novel approximate analytical solutions to compute the time-dependent internal stress state throughout the pipe thickness within the framework of nonlinear viscoelasticity theory. The structures considered are thick, multilayered anisotropic infinitive long cylinders subjected to axisymmetric mechanical loading. Under such conditions there is an exact elastic solution which naturally satisfies equilibrium, strain-displacement, compatibility and boundary conditions for the stated constitutive equations and loading. Due to the continuous stress variations throughout the cylinder thickness, the proposed nonlinear viscoelastic solution assumes the averaged stress state to calculate the nonlinear elastic and viscoelastic factors in each

layer. Furthermore the solution is obtained assuming that the creep strains, within each layer, are constant through the thickness. The proposed algorithm converges to the exact solution when the number of layers is artificially increased. For the linear viscoelastic case the proposed solution proved to match the exact known solution for isotropic viscoelastic materials. Finally several invented cases are run to illustrate the importance of the viscoelasticity phenomenon on the internal stress field throughout thick laminated cylinders.

KEYWORDS: Polymer–matrix composites (PMCs); Creep; Elasticity; Analytical modelling; Durability.

INTRODUCTION

The hollow cylinders or cylinders are very common structural elements, used in many applications including trusses, hoses, piping systems and drive shafts. The effort to improve oil production riser performance lead to the possible use of risers made of polymer matrix composites to bring the oil to surface platforms in the offshore exploration at waster depth of 2 km or more. Consequently the increasing use of polymer matrix composites in civil engineering applications has renewed interest in problems of stress analysis of cylindrical laminated composite structures.

Many analytical works about stress analysis of composite cylindrical shells have been done during the past years. This is related with the increase use of composite shells in many applications, such as civil engineering structures and aeronautical industry. The

static behaviour of thin shell panels has been investigated by using two-dimensional shell theories based on the Love-Kirchhoff hypotheses. Chandrashekhara and Kumar [1] presented and assessed these shell theories. The laminated shell theories provide an accurate solution for thin-walled cylinders but for thick-walled cylinders elasticity solutions are required for an accurate determination of the three-dimensional stress states.

The nonlinear viscoelastic analysis of thick laminated composites, using the Schapery nonlinear visceolastic constitutive equations [2], has been preformed, essentially, using finite elements (FE) formulations whether using a ply-by-ply classical approach [3] or using a more sophisticated approach based on multi-scale approach [4] [5].

The laminated cylinder is one of a very few structural cases for which an exact elasticity solution is available. The analytical solution for multilayered cylinders is described in detail by Herakovich [6]. This is based on the early works of Lekhnitskii [7] and Pagano [8] among others. Based on this elastic solution a novel nonlinear viscoelastic analytical approximate solution was developed, using the Schapery [2] non-linear viscoelastic constitutive equations, to compute the stress state of nonlinear viscoelastic polymer matrix fiber reinforced laminated thick cylinders. The present solution considers that the material is linear elastic in the fiber direction and nonlinear elastic-viscoelastic in transverse and shear directions to the fibre. It is also assumed that the material is transversely isotropic. Since the stress state changes continuously throughout each layer thickness, the averaged stress state is used when computing the nonlinear elastic and viscoelastic factors for each layer. Furthermore the solution is obtained assuming that the creep strains, within each layer, are constant through the thickness.

The present analytical approximate solution converges to the exact solution when the number of layers is artificially increased. The proposed approximated solution matches the exact known solution for the pressurization of a compressible linear viscoelastic isotropic cylinder constrained by an elastic case.

Finally several invented cases are run to simulate the mechanical behaviour of a nonlinear viscoelastic T300/5208 [9] composite cylinder under internal pressure, external pressure and axial force. These cases are used to demonstrate the importance of the viscoelasticity effect over the time-dependent internal stress field evolution throughout thick laminated cylinders.

APPROXIMATE NON-LINEAR VISCOELASTIC SOLUTION

Few composite structural configurations have an exact elasticity solution and the laminated circular cylinder is one of those cases. The exact elasticity solution for a long, circular cylinder made from a homogeneous, monoclinic layer and subjected to axisymmetric mechanical loading is well established [6]. In this case the mechanical loads are applied axisymmetrically at the ends and uniformly and axisymmetrically along the length. This exact elastic solution satisfies equilibrium, strain-displacement, compatibility and boundary conditions for the stated constitutive equations and loading.

For a long axisymmetric cylinder under the prescribed loading, i.e. loaded uniformly along its length, the stresses are independent of x and θ (see Figure 1). Hence the partial differential equilibrium equation reduces to ordinary in r only,

$$\begin{cases} \dfrac{\partial \sigma_r}{\partial r} + \dfrac{\sigma_r - \sigma_\theta}{r} = 0 \\ \dfrac{\partial \tau_{\theta r}}{\partial r} + \dfrac{2\tau_{\theta r}}{r} = 0 \\ \dfrac{\partial \tau_{xr}}{\partial r} + \dfrac{\tau_{xr}}{r} = 0 \end{cases}. \tag{1}$$

For a hollow cylinder subjected to normal stresses on its internal surface and on external surface the boundary conditions are (see Figure 1)

$$\begin{cases} \sigma_r(R_i) = -P_i \\ \tau_{\theta r}(R_i) = 0 \\ \tau_{xr}(R_i) = 0 \end{cases} \text{ and } \begin{cases} \sigma_r(R_e) = -P_e \\ \tau_{\theta r}(R_e) = 0 \\ \tau_{xr}(R_e) = 0 \end{cases}, \tag{2}$$

where R_i and R_e represent the internal and the external radius, respectively and P_i and P_e represent the internal and external pressure, respectively.

Integration of the last two equations using the shear stress boundary conditions gives the zero shear stress, i.e.

$$\begin{cases} \tau_{\theta r} = 0 \\ \tau_{xr} = 0 \end{cases}. \tag{3}$$

The most general displacements for the problem under consideration are,

$$\begin{cases} u = u(x,r) & \text{–axial} \\ v = v(x,r) & \text{–tangential} \\ w = w(r) & \text{–radial} \end{cases}. \tag{4}$$

The reduced strain-displacement equations for the axisymmetric cylinder loaded uniformly along its length are

$$\begin{cases} \varepsilon_x = \dfrac{\partial u}{\partial x} \\ \varepsilon_\theta = \dfrac{w}{r} \\ \varepsilon_r = \dfrac{\partial w}{\partial r} \\ \gamma_{\theta r} = \dfrac{\partial v}{\partial r} - \dfrac{v}{r} \\ \gamma_{xr} = \dfrac{\partial u}{\partial r} \\ \gamma_{x\theta} = \dfrac{\partial v}{\partial x} \end{cases}, \tag{5}$$

Three of the equations of compatibility are satisfied identically for the above strains. The remaining three are

$$\begin{cases} \dfrac{d^2\varepsilon_x}{\partial r^2} = 0 \\ \dfrac{1}{r}\dfrac{d\varepsilon_x}{dr} = 0, \\ \dfrac{1}{2}\dfrac{d}{dr}\left[\dfrac{1}{r}\dfrac{d}{dr}(r\gamma_{x\theta})\right] = 0 \end{cases} \tag{6}$$

Integration of the first two show that the axial strain is constant in the layer,

$$\varepsilon_x = \varepsilon_x^{\,0} \tag{7}$$

An orthotropic viscoelastic layer the constitutive equations in principal material (1,2,3) coordinates (see Figure 1) are,

$$\begin{bmatrix} \sigma_1 \\ \sigma_2 \\ \sigma_3 \\ \tau_{23} \\ \tau_{31} \\ \tau_{12} \end{bmatrix} = \begin{bmatrix} C_{11} & C_{12} & C_{13} & 0 & 0 & 0 \\ C_{12} & C_{22} & C_{23} & 0 & 0 & 0 \\ C_{13} & C_{23} & C_{33} & 0 & 0 & 0 \\ 0 & 0 & 0 & C_{44} & 0 & 0 \\ 0 & 0 & 0 & 0 & C_{55} & 0 \\ 0 & 0 & 0 & 0 & 0 & C_{66} \end{bmatrix} \left\{ \begin{bmatrix} \varepsilon_1 \\ \varepsilon_2 \\ \varepsilon_3 \\ \gamma_{23} \\ \gamma_{31} \\ \gamma_{12} \end{bmatrix} - \begin{bmatrix} \varepsilon_1 \\ \varepsilon_2 \\ \varepsilon_3 \\ \gamma_{23} \\ \gamma_{31} \\ \gamma_{12} \end{bmatrix}^{creep} \right\}. \tag{8}$$

The elastic-viscoelastic constitutive equations in the global cylindrical (x,θ,r) coordinated for this orthotropic layer at a fiber angle ϕ to the axial x-direction are given by

$$\begin{bmatrix}\sigma_x\\ \sigma_\theta\\ \sigma_r\\ \tau_{\theta r}\\ \tau_{xr}\\ \tau_{x\theta}\end{bmatrix}=\begin{bmatrix}\bar{C}_{11} & \bar{C}_{12} & \bar{C}_{13} & 0 & 0 & \bar{C}_{16}\\ \bar{C}_{12} & \bar{C}_{22} & \bar{C}_{23} & 0 & 0 & \bar{C}_{26}\\ \bar{C}_{13} & \bar{C}_{23} & \bar{C}_{33} & 0 & 0 & \bar{C}_{36}\\ 0 & 0 & 0 & \bar{C}_{44} & \bar{C}_{45} & 0\\ 0 & 0 & 0 & \bar{C}_{45} & \bar{C}_{55} & 0\\ \bar{C}_{16} & \bar{C}_{26} & \bar{C}_{36} & 0 & 0 & \bar{C}_{66}\end{bmatrix}\left\{\begin{bmatrix}\varepsilon_x\\ \varepsilon_\theta\\ \varepsilon_r\\ \gamma_{\theta r}\\ \gamma_{xr}\\ \gamma_{x\theta}\end{bmatrix}-\begin{bmatrix}\varepsilon_x\\ \varepsilon_\theta\\ \varepsilon_r\\ \gamma_{\theta r}\\ \gamma_{xr}\\ \gamma_{x\theta}\end{bmatrix}^{creep}\right\}. \tag{9}$$

where $\bar{C}_{ij}$ are given by transformation equations [2].

By using the constitutive, equilibrium and strain-displacement equations the following axial and tangential displacements, respectively, are obtained

$$\begin{cases}u(x,r)=\varepsilon_x{}^0 x\\ v(x,r)=\gamma^0 xr\end{cases}. \tag{10}$$

For the radial displacement the following second order differential equation is obtained by assuming that the creep strain is constant through the layer thickness, i.e. in radial direction,

$$\frac{dw^2}{dr^2}+\frac{1}{r}\frac{dw}{dr}-\frac{\bar{C}_{22}}{\bar{C}_{33}}\frac{w}{r^2}=\frac{1}{\bar{C}_{33}}\left[\frac{\left(\bar{C}_{12}-\bar{C}_{13}\right)\varepsilon_x{}^0+\sum_{creep}}{r}+\left(\bar{C}_{26}-2\bar{C}_{36}\right)\gamma^0\right]. \tag{11}$$

where

$$\sum_{creep}=\left(\bar{C}_{k3}-\bar{C}_{k2}\right)\varepsilon_k^{\,creep},\quad k=1,2,\ldots,6 \tag{12}$$

The solution of Equation (11) is

$$w(r) = A_1 r^{\chi} + A_2 r^{-\chi} + \frac{(\bar{C}_{12} - \bar{C}_{13})}{(\bar{C}_{33} - \bar{C}_{22})} \varepsilon_x{}^0 r + \frac{(\bar{C}_{26} - 2\bar{C}_{36})}{(4\bar{C}_{33} - \bar{C}_{22})} \gamma^0 r^2 + \frac{\sum_{creep}}{(\bar{C}_{33} - \bar{C}_{22})} r \,, \tag{13}$$

where

$$\chi = \sqrt{\frac{\bar{C}_{22}}{\bar{C}_{33}}} \,. \tag{14}$$

If the layer is isotropic or transversely isotropic then $\bar{C}_{22} = \bar{C}_{33}, \bar{C}_{12} = \bar{C}_{13}, \bar{C}_{i6} = 0$ and the Equation (11) takes the form

$$\frac{dw^2}{dr^2} + \frac{1}{r}\frac{dw}{dr} - \frac{w}{r^2} = \frac{1}{r\bar{C}_{33}} \sum_{creep} \quad , \tag{15}$$

which has the solution

$$w(r) = A_1 r + A_2 \frac{1}{r} + \frac{\sum_{creep}}{4\bar{C}_{33}} (2\ln r - 1) r \,. \tag{16}$$

Let us assume that the material is linear-elastic in fibre direction and all nonlinear and viscoelastic response is transverse to the fibers or in shear. If we assume that the material can be treated as being isotropic in the 2,3 plane, then using the Schapery [2] analytical approach for creep we obtain

$$\begin{bmatrix}\varepsilon_1\\ \varepsilon_2\\ \varepsilon_3\\ \gamma_{23}\\ \gamma_{31}\\ \gamma_{12}\end{bmatrix}^{creep} = \begin{bmatrix} 0 \\ g_{1,22}\int_0^t \Delta S_{22}(\psi-\psi')\frac{d\left(g_{2,22}\sigma_2(\tau)\right)}{d\tau}d\tau + g_{1,23}\int_0^t \Delta S_{23}(\psi-\psi')\frac{d\left(g_{2,23}\sigma_3(\tau)\right)}{d\tau}d\tau \\ g_{1,22}\int_0^t \Delta S_{22}(\psi-\psi')\frac{d\left(g_{2,22}\sigma_3(\tau)\right)}{d\tau}d\tau + g_{1,23}\int_0^t \Delta S_{23}(\psi-\psi')\frac{d\left(g_{2,23}\sigma_3(\tau)\right)}{d\tau}d\tau \\ g_{1,44}\int_0^t \Delta S_{44}(\psi-\psi')\frac{d\left(g_{2,44}\sigma_4(\tau)\right)}{d\tau}d\tau \\ g_{1,66}\int_0^t \Delta S_{55}(\psi-\psi')\frac{d\left(g_{2,66}\sigma_5(\tau)\right)}{d\tau}d\tau \\ g_{1,66}\int_0^t \Delta S_{66}(\psi-\psi')\frac{d\left(g_{2,66}\sigma_6(\tau)\right)}{d\tau}d\tau \end{bmatrix} \quad (17)$$

where

$$\psi = \int_0^t \frac{d\tau'}{a_{\sigma,mn}} \quad , \quad \psi' = \int_0^\tau \frac{d\tau'}{a_{\sigma,mn}} \quad (18)$$

where the nonlinear parameters $g_{1,mn}, g_{2,mn}, a_{\sigma,mn}$ are stress dependent (of some stress invariant). Due the restriction imposed on the creep strain, i.e. constancy in radial direction, the creep strains are calculated using the averaged stress state in the layer.

If the kernels in Equation (17) are represented by a Prony series as

$$\Delta S_{mn}(t) = \sum_{i=1}^{N} S_{i,mn}\left(1-e^{-\lambda_{i,mn}t}\right) \quad (19)$$

and the Poisson coefficients ν_{12} and ν_{23} are assumed constant, the creep strains at each instant *t*, after integration, can be described by the following equations

$$\begin{bmatrix}\varepsilon_1\\ \varepsilon_2\\ \varepsilon_3\\ \gamma_{23}\\ \gamma_{31}\\ \gamma_{12}\end{bmatrix}^{creep}=\begin{bmatrix}0\\ g_{1,22}\left[\sum_{i=1}^{N}\varepsilon_{i,22}\left(g_{2,22},a_{\sigma,22},\sigma_2,t\right)-\nu_{23}\sum_{i=1}^{N}\varepsilon_{i,22}\left(g_{2,22},a_{\sigma,22},\sigma_3,t\right)\right]\\ g_{1,22}\left[\sum_{i=1}^{N}\varepsilon_{i,22}\left(g_{2,22},a_{\sigma,22},\sigma_3,t\right)-\nu_{23}\sum_{i=1}^{N}\varepsilon_{i,22}\left(g_{2,22},a_{\sigma,22},\sigma_2,t\right)\right]\\ g_{1,22}\left[\sum_{i=1}^{N}\varepsilon_{i,22}\left(g_{2,22},a_{\sigma,22},\sigma_4,t\right)\right]\left(2+2\nu_{23}\right)\\ g_{1,66}\left[\sum_{i=1}^{N}\varepsilon_{i,66}\left(g_{2,66},a_{\sigma,66},\sigma_5,t\right)\right]\\ g_{1,66}\left[\sum_{i=1}^{N}\varepsilon_{i,66}\left(g_{2,66},a_{\sigma,66},\sigma_6,t\right)\right]\end{bmatrix}. \quad (20)$$

where the internal strains $\varepsilon_{i,mn}$ are obtained using the following recursive formula (see appendix I)

$$\varepsilon_{i,mn}\left(g_{2,mn},a_{\sigma,mn},\sigma_{j+1},t_{j+1}\right)=S_{i,mn}g_{2,mn}\sigma_{j+1}\left(1-e^{-\frac{\lambda_{i,mn}}{a_{\sigma,mn}}\Delta t}\right)+e^{-\frac{\lambda_{i,mn}}{a_{\sigma,mn}}\Delta t}\varepsilon_{i,mn}\left(g_{2,mn},a_{\sigma,mn},\sigma_j,t_j\right) \quad (21)$$

The restriction introduced by considering the creep strains constant in radial direction allows the analytical solution of axial displacements. Still this approximation can be used in moderately thick layers as it will be shown in the next section. Furthermore the solution converges to the exact solution when the number of layers is artificially increased.

The filament wound structures are assumed to have a wind angle of ϕ. In a multi-layered cylinder, each layer may have each own wind angle. In the present study are considered cylindrical shells made of *M* orthotropic plies with different wind angles.

The solution for a laminated, multilayered cylinder proceeds directly from the solution for a single-layer. The requirements are the stress and strain continuity at the layer interfaces.

In this case there are 4*M* unknowns ($\varepsilon_x^{\,0}, \gamma^0, A_1, A_2$) for each layer. However due to the continuity of displacements between layers one must have $\varepsilon_x^{\,0}$ and γ^0 constants throughout the cylinder thickness. Therefore the number of unknowns reduces to 2*M*+2. The corresponding equations are 2*(M*-1*)* continuity equations for radial displacements and stresses,

$$w^{(p)} = w^{(p+1)} \quad \text{and} \quad \sigma_r^{\,(p)} = \sigma_r^{\,(p+1)} \quad \text{at interfaces } p = 1, \ldots, M-1, \tag{22}$$

two boundary surface conditions,

$$\sigma_r\left(R_e\right) = -P_e \quad \text{and} \quad \sigma_r\left(R_i\right) = -P_i, \tag{23}$$

and two equilibrium equations, axial force

$$P = 2\pi \int_{R_{out}}^{R_{in}} \sigma_x r dr\,, \tag{24}$$

and torque

$$T = 2\pi \int_{R_{out}}^{R_{in}} \tau_{r\theta} r^2 dr\,, \tag{25}$$

which gives exactly 2*M*+2 independent equations.

Finally since it is assumed that the material is linear-elastic in fibre direction and all nonlinear response is transverse to the fibers or in shear, the elastic nonlinear compliance in principal material (1,2,3) coordinates is given by

$$[S]=\begin{bmatrix} S_{11} & -\nu_{12}S_{11} & -\nu_{12}S_{11} & 0 & 0 & 0 \\ -\nu_{12}S_{11} & S_{22}g_{0,22} & -\nu_{23}S_{22}g_{0,22} & 0 & 0 & 0 \\ -\nu_{12}S_{11} & -\nu_{23}S_{22}g_{0,22} & S_{22}g_{0,22} & 0 & 0 & 0 \\ 0 & 0 & 0 & 2(1+\nu_{23})S_{22}g_{0,22} & 0 & 0 \\ 0 & 0 & 0 & 0 & S_{66}g_{0,66} & 0 \\ 0 & 0 & 0 & 0 & 0 & S_{66}g_{0,66} \end{bmatrix}, \tag{26}$$

where $g_{0,22}, g_{0,66}$ are the elastic the nonlinear parameters that are stress dependent (of some stress invariant). The respective stiffness matrix is immediately obtained by matrix inversion. This algorithm was programmed into a FORTRAN computer code named as RESFLU.

EXACT ANALYTICAL SOLUTION FOR A LINEAR VISCOELASTIC CYLINDER

Christensen [10] presented an exact solution for the pressurization of a compressible linear viscoelastic cylinder constrained by an elastic case, considering sufficient long cylinders such that plane strain conditions can be assumed. The solution also assumes that the Poisson coefficient ν is constant. Using the Prony series to represent the shear viscoelastic relaxation,

$$G(t)=G_0+\sum_{i=1}^{N}G_i e^{-t/\tau_i} \tag{27}$$

The *s* multiplied Laplace transform is given by

$$s\bar{G}(s)=\frac{A(s)}{\prod_{i=1}^{N}\left(s+\tau_i^{-1}\right)}=\frac{A(s)}{B(s)} \tag{28}$$

The solution, after Laplace transform inversion, gives

$$\sigma_r(r,t)=P_i\sum_{i=1}^{N}\frac{\left[C(a_i)-\left(R_e^{\,2}/r^2\right)D(a_i)\right]e^{-a_i t}}{\lim_{s\to a_i}\left[F(s)/(s-a_i)\right]} \tag{29}$$

$$\sigma_\theta(r,t)=P_i\sum_{i=1}^{N}\frac{\left[C(a_i)+\left(R_e^{\,2}/r^2\right)D(a_i)\right]e^{-a_i t}}{\lim_{s\to a_i}\left[F(s)/(s-a_i)\right]} \tag{30}$$

$$\sigma_x(r,t)=P_i\sum_{i=1}^{N}\frac{2\nu C(a_i)e^{-a_i t}}{\lim_{s\to a_i}\left[F(s)/(s-a_i)\right]} \tag{31}$$

where

$$C(s)=-K\cdot B(s)+A(s) \tag{32}$$

$$D(s)=(1-2\nu)K\cdot B(s)+A(s) \tag{33}$$

$$\begin{aligned}F(s)&=s\left\{K\cdot B(s)-A(s)+\left(R_e^{\,2}/R_i^{\,2}\right)\left[(1-2\nu)K\cdot B(s)+A(s)\right]\right\}\\&=\kappa(s-a_1)(s-a_2)\cdots(s-a_N)\end{aligned} \tag{34}$$

where κ is a constant and a_i are the roots of $F(s)$ and the integer N the number of terms of the representation given by (27) and

$$K=\frac{E_c h}{2R_e\left(1-\nu_c^{\,2}\right)}, \tag{35}$$

where E_c and ν_c are the elastic modulus and Poisson coefficient of the steel case, respectively, and h is the case thickness.

In order to verify the present algorithm an example was run to simulate an internal pressurized (100MPa) viscoelastic cylinder (polymer) with an internal radius (R_i) of 600mm and an external radius of 798mm constrained by an elastic case (steel) 2mm thick, i.e. the composite cylinder has an external radius (R_e) of 800mm. The cylinder is considered sufficient long such that plain strain conditions can be assumed. The properties considered for the steel case were $E_c = 205\text{MPa}$ and $\nu_c = 0.3$. The polymer has a Poisson coefficient $\nu = 0.3$ and the shear relaxation modulus data is given in Table I.

The equivalent shear creep compliance, given by equation 36, data used in RESFLU is given in Table II. In the present algorithm the plane strain solution corresponds to impose an axial strain restriction. The results of RESFLU follow quite closed Christensen [10] solution as depicted in figures 2 to 4.

$$S_{12}(t) = S_0 + \sum_{i=1}^{N} S_i \left(1 - e^{-\lambda_i t}\right). \tag{36}$$

The results are in an excellent agreement with exact linear viscoelastic solution.

NONLINEAR VISCOELASTIC CYLINDERS

The simulations which follow are based on the present algorithm, RESFLU. The cases presented are invented without any experimental results, just for illustrative purposes. It is simulated the mechanical behaviour of a composite cylinder under internal pressure, external pressure and axial force. For this purpose it is considered a carbon fibre reinforced laminated T300/5208 [9] cylinder with the staking sequences of [45/-45/-

45/45] and [54/-54/-54/54]. The material properties, based on the results published by Tuttle and Brinson (1986) are described in Tables III-V. The cylinder with closed ends has an inner radius R_i=200mm and a inner radius to thickness ratio of R_i /h of 100, 10, 5 and 2.

The octahedral shear stress in the matrix, accordingly with Lou and Schapery [11] stress, is given by

$$\tau_{oct} = \frac{1}{3}\sqrt{\left(\sigma_1^{\,m} - \sigma_2^{\,m}\right)^2 + \left(\sigma_1^{\,m} - \sigma_3^{\,m}\right)^2 + \left(\sigma_2^{\,m} - \sigma_3^{\,m}\right)^2 + 6\left(\tau_{23}^{\,m}\right)^2 + 6\left(\tau_{31}^{\,m}\right)^2 + 6\left(\tau_{12}^{\,m}\right)^2}\,, \tag{37}$$

where

$$\begin{bmatrix} \sigma_1^{\,m} \\ \sigma_2^{\,m} \\ \sigma_3^{\,m} \\ \tau_{23}^{\,m} \\ \tau_{31}^{\,m} \\ \tau_{12}^{\,m} \end{bmatrix} = \begin{bmatrix} \frac{E_m}{E_{11}} & \nu_m - \frac{E_m}{E_{11}}\nu_{12} & 0 & 0 & 0 & 0 \\ 0 & 1 & 0 & 0 & 0 & 0 \\ 0 & 0 & 1 & 0 & 0 & 0 \\ 0 & 0 & 0 & 1 & 0 & 0 \\ 0 & 0 & 0 & 0 & 1 & 0 \\ 0 & 0 & 0 & 0 & 0 & 1 \end{bmatrix} \begin{bmatrix} \sigma_1 \\ \sigma_2 \\ \sigma_3 \\ \tau_{23} \\ \tau_{31} \\ \tau_{12} \end{bmatrix}.$$

Nonlinearity arises also as a consequence of the deformations, provoking internal volume change as well as the angles of layers. The radius $r_j^{\,0}$ in the unloaded state can be found to vary in function of the respective hoop strain as

$$r_j = r_j^{\,0}\left(1+\varepsilon_\theta\right). \tag{38}$$

The angle ϕ of each layer change in function of the respective averaged axial and hoop strain in the same manner used by Dillard [12] for the laminated composites,

$$\operatorname{tg}\phi = \operatorname{tg}\phi^0 \frac{\left(1+\varepsilon_\theta\right)}{1+\varepsilon_x + \gamma_{x\theta}\operatorname{tg}\phi^0}. \tag{39}$$

where ϕ^0 represents the layer angle in the unloaded state and $\varepsilon_x, \varepsilon_\theta, \gamma_{x\theta}$ represent the axial, tangential and shear strains.

In the present case it was also assumed that the viscoelastic behaviour under compression is symmetrical of the tensile viscoelastic behaviour which may be not the case in real material systems.

The loading conditions used in this study are described briefly as follows.

Internal pressure

The internal pressure was chosen, considering the thin cylinder theory, to result into a hoop stress of 100MPa as depicted in figure 5,

$$\begin{aligned}\sigma_\theta &= p_i \frac{R_i}{R_e - R_i} = 100\text{MPa}, \\ \sigma_x &= p_i \frac{\pi R_i^{\,2}}{\pi\left(R_e^{\,2} - R_i^{\,2}\right)} = p_i \frac{R_i^{\,2}}{2\left(R_e - R_i\right)\left(R_e + R_i\right)/2} \approx p_i \frac{R_i}{2\left(R_e - R_i\right)} = 50\text{MPa}\end{aligned}. \qquad (40)$$

External pressure

The external pressure was chosen, considering the thin cylinder theory, to result into a hoop stress of 100MPa as depicted in figure 6,

$$\begin{aligned}\sigma_\theta &= p_e \frac{R_e}{R_e - R_i} = -100\text{MPa}, \\ \sigma_x &= p_e \frac{\pi R_e^{\,2}}{\pi\left(R_e^{\,2} - R_i^{\,2}\right)} = p_e \frac{R_e^{\,2}}{2\left(R_e - R_i\right)\left(R_e + R_i\right)/2} \approx p_e \frac{R_e}{2\left(R_e - R_i\right)} = -50\text{MPa}\end{aligned}. \qquad (41)$$

Axial loading

The axial load was chosen, considering the thin cylinder theory, to result into an axial compressive stress of 100MPa as depicted in figure 7,

$$\sigma_x = \frac{F_x}{\pi\left(R_e^{\,2} - R_i^{\,2}\right)} = -100\text{MPa}\,. \qquad (42)$$

RESULTS AND DISCUSSION

The reference creep strain values for thin cylinders were obtained from the algorithm LAMLFU [13], which extends the classical laminate theory to include the non-linear Schapery viscoelastic model. For each loading case follows the presentation and discussion of the results.

Internal pressure

For this load case two different staking sequences were simulated [45/-45/-45/45] and [54/-54/-54/54]. The purpose was to illustrate the staking influence on the creep evolution. The first case clearly shows a strong dependence on the viscoelastic matrix exhibiting high creep extensions for all inner radius to thickness ratios R_i/h considered, as depicted in figure 8. However the second staking sequence shows little creep extensions except for the thicker case which exhibits a high compressive axial creep deformation, as depicted in figure 9. The hoop and axial stresses also show large changes for the thicker cases, after 10^5min, as depicted in figures 10 and 11. This represents an increase of 38% for the hoop stress and 47% for the axial stress in the inner side of the cylinder with R_i/h=2. In the case of cylinder with R_i/h=5 the increase is just 4% for both stresses in the inner side.

External pressure

In this case the [54/-54/-54/54] staking sequence shows also a week dependence on the viscoelastic matrix, as depicted in figure 12. However the strain deformation depends strongly on the cylinder thickness. Furthermore the cylinder shows small time-dependent stress changes, as depicted in figures 13 and 14, due to the viscoelastic effect, when compared against the internal pressure case.

Axial loading

This last case exhibits an external axial and hoop strains strongly affected by viscoelastic nature of the matrix, with no significant thickness influence, as depicted in figure 15. However the stresses variations due to the viscoelastic effect are significantly larger than in the internal pressure case, as shown throughout figures 16-21. The increase, after 10^5 min, of the axial stress in the inner side of the cylinder was more than 200% for the R_i/h=2 and R_i/h=5 cylinders. The maximum shear stress also presents an increase of more than 100% in the outer side of the cylinders for the same inner radius to thickness ratios. Furthermore the maximum radial stress increases more than 200%.

The computed reference strains, given by LAMFLU, match the computed strains by RESFLU for the R_i/h=100 cylinders which is a good indication on the quality of the RESFLU results for the nonlinear viscoelastic calculations. All simulated cases show the need to compute the time-dependent stress state throughout the thickness, especially in the presence of thick walled cylinders. The external pressure loading case displayed the least time-dependent stress variation. By opposite the axial compressive loading case has shown the most critical stress variation. Generally the internal stress

redistributions due to the viscoelastic nature of the matrix lead, after a certain amount of time, to stress states which in some cases are far from the initial computed (elastic) stress state. This phenomenon, for sure, can lead to premature failures. Therefore careful time-dependent stress analyze should be performed in the presence of viscoelastic thick walled cylinders. The present approach is a first step towards the long-term failure prediction of nonlinear viscoelastic multilayered composite cylinders under constant or cyclic loading.

CONCLUSIONS

This work presents a novel analytical approach to calculate the time-dependent stress-strain state in nonlinear viscoelastic multilayered composite cylinders. The solution is possible when some restrictions in each ply are imposed, i.e. the creep strains are assumed constant and the nonlinear elastic and viscoelastic factors are computed using the averaged stress state in each layer. The exact solution can be found when the number of layers, artificially introduced, increases to infinity. The proposed solution, obtained using few layers, matched the exact known solution for the pressurization of a compressible linear viscoelastic cylinder constrained by an elastic case.

Invented cases are run to simulate the mechanical behaviour of a T300/5208 nonlinear viscoelastic multilayered composite cylinder under internal pressure, external pressure and axial force. These cases are used to demonstrate the importance of the viscoelasticity effect over the time-dependent internal stress field evolution throughout thick laminated cylinders. In some cases, given enough time, the stress states evolve

into stress states which, in some cases, are far from the initial computed (elastic) stress state.

ACKNOWLEDGMENTS

The research hereby presented was supported by Fundação para a Ciência e Tecnologia (Ministério da Ciência e do Ensino Superior) through project POCTI/EME/44644/2002.

APPENDIX I

In order to eliminate the Volterra-type integrals, the transverse and shear compliance are expressed using Prony series, as Gramoll [14] and Czyz [15] have already discussed. Then the creep strain can be described by

$$\varepsilon_{mn}^{\ creep}(t) = g_{1,mn}\sum_{i=1}^{N}\varepsilon_{i,mn}(t) \tag{I.1}$$

where

$$\varepsilon_{i,mn}(t) = S_{i,mn}\int_0^t\left(1-e^{-\lambda_{i,mn}(\psi-\psi')}\right)\frac{dg_{2,mn}\sigma(\tau)}{d\tau}d\tau \tag{I.2}$$

The previous equation can be integrated

$$\varepsilon_{i,mn}(t_j) = \tilde{g}_{i,mn}(\sigma_j) - e^{-\lambda_{i,mn}\nu(t_j)}\int_0^{t_j} e^{\lambda_{i,mn}\nu(\tau)}\frac{d\tilde{g}_{i,mn}(\sigma)}{d\tau}d\tau \tag{I.3}$$

with

$$\tilde{g}_{i,mn}(\sigma) = S_{i,mn}\, g_{2,mn}\,\sigma$$

and

$$v(t)=\int_0^t \frac{d\tau'}{a_{\sigma,mn}}$$

Let us now calculate $\varepsilon_{i,mn}(t_{j+1})$ for the time t_{j+1} based on the knowledge of the value of $\varepsilon_{i,mn}(t_j)$ at the time t_j.

$$\varepsilon_{i,mn}(t_{j+1})=\tilde{g}_{i,mn}(\sigma_{j+1})-e^{-\lambda_{i,mn}v(t_{j+1})}\left\{\int_0^{t_j} e^{\lambda_{i,mn}v(\tau)}\frac{d\tilde{g}_{i,mn}(\sigma)}{d\tau}d\tau+\int_{t_j}^{t_{j+1}} e^{\lambda_{i,mn}v(\tau)}\frac{d\tilde{g}_{i,mn}(\sigma)}{d\tau}d\tau\right\} \tag{I.4}$$

Therefore

$$\varepsilon_{i,mn}(t_{j+1})=\tilde{g}_{i,mn}(\sigma_{j+1})-e^{-\lambda_{i,mn}\left[v(t_{j+1})-v(t_j)\right]}\left[\tilde{g}_{i,mn}(\sigma_j)-\varepsilon_i(t_j)\right]-e^{-\lambda_{i,mn}v(t_{j+1})}\int_{t_j}^{t_{j+1}} e^{\lambda_{i,mn}v(\tau)}\frac{d\tilde{g}_{i,mn}(\sigma)}{d\tau}d\tau \tag{I.5}$$

Noting the following relationships

$$-\lambda_{i,mn}\left[v(t_{j+1})-v(\tau)\right]=-\lambda_{i,mn}\int_\tau^{t_{j+1}}\frac{d\tau'}{a_{\sigma,mn}}=\frac{-\lambda_{i,mn}}{a_{\sigma,mn}(\sigma_{j+1})}(t_{j+1}-\tau)\quad,\quad t_j\le\tau\le t_{j+1} \tag{I.6}$$

and

$$-\lambda_{i,mn}\left[v(t_{j+1})-v(t_j)\right]=-\lambda_{i,mn}\int_{t_j}^{t_{j+1}}\frac{d\tau'}{a_{\sigma,mn}}=\frac{-\lambda_{i,mn}}{a_{\sigma,mn}(\sigma_{j+1})}(t_{j+1}-t_j) \tag{I.7}$$

Finally the equation (I.5) can be integrated

$$e^{-\lambda_{i,mn}v(t_{j+1})}\int_{t_j}^{t_{j+1}} e^{\lambda_{i,mn}v(\tau)}\frac{d\tilde{g}_{i,mn}(\sigma)}{d\tau}d\tau=\int_{t_j}^{t_{j+1}} e^{-\lambda_{i,mn}\left[v(t_{j+1})-v(\tau)\right]}\frac{d\tilde{g}_{i,mn}(\sigma)}{d\tau}d\tau=e^{-\lambda_{i,mn}\frac{\Delta t}{a_{\sigma,mn}(\sigma_{j+1})}}\left[\tilde{g}_{i,mn}(\sigma_{j+1})-\tilde{g}_i(\sigma_j)\right] \tag{I.8}$$

with $\Delta t=t_{j+1}-t_j$

Replacing this result (I.8) into equation (I.5) the recursive formula is obtained

$$\varepsilon_{i,mn}\left(t_{j+1}\right)=\tilde{g}_{i,mn}\left(\sigma_{j+1}\right)-e^{-\lambda_{i,mn}\frac{\Delta t}{a_{\sigma,mn}\left(\sigma_{j+1}\right)}}\left[\tilde{g}_{i,mn}\left(\sigma_{j+1}\right)-\varepsilon_{i}\left(t_{j}\right)\right] \quad \text{(I.9)}$$

REFERENCES

[1] Chandrashekhara K. and Pavan Kumar DVTG. Assessment of shell theories for the static analysis of cross-ply laminated circular cylindrical shells. Thin-Walled Structures, 1995;22(4):291-318.

[2] Schapery, R. A. On the Characterization of Nonlinear Viscolelastic Materials. Polymer Engineering and Science, 1969; 9(4):295-310.

[3] Kennedy, Timothy C., Wang, Min. Three-dimensional, nonlinear viscoelastic analysis of laminated composites. Journal of Composite Materials, 1994;28 (10):902-925.

[4] Muliana A.H., Haj-Ali R.M. Analysis for creep behavior and collapse of thick-section composite structures. Composite Structures, 2006;73 (3):331-341.

[5] Haj-Ali R., Muliana A. A micro-to-meso sublaminate model for the viscoelastic analysis of thick-section multi-layered FRP composite structures. Mechanics of Time-Dependent Materials, 2008;12 (1):69-93.

[6] Herakovich C.T. Mechanics of Fibrous Composites: John Wiley & Sons 1998.

[7] Lekhnitskii S. G. Theory of Elasticity of an Anisotropic Body: Mir Publishers 1981.

[8] Pagano N. J.,Whitney J. M.. Geometric Design of Composite Cylindrical Characterization Specimens. J. Composite Materials, 1970;4:360-378.

[9] Tuttle ME, Brinson HF. Prediction of the long-term creep compliance of general composite laminates. Exp Mech, 1986;26(1):89-102.

[10] Christensen R. M.. *Theory of Viscoelasticity*. Dover Publications 1982.

[11] Lou Y.C., Schapery R.A. Viscoelastic Characterization of a Nonlinear Fiber-Reinforced Plastic. Journal of Composite Materials,1971; 5:208 - 234.

[12] Dillard DA. Creep and creep rupture of laminated graphite/epoxy composites. Ph.D. Thesis, Va. Tech. 1980.

[13] Guedes, R. M., Marques, A. T. and Cardon, A. H. Analytical and Experimental Evaluation of Nonlinear Viscoelastic-Viscoplastic Composite Laminates under

Creep, Creep-Recovery, Relaxation and Ramp Loading. Mechanics of Time-Dependent Materials, 1998;2: 113–128.

[14] Gramoll, K. C., Dillard D. A., Brinson H. F. A Stable Numerical Solution Method for In-plane Loading of Nonlinear Viscoelastic Laminated Orthotropic Materials. Composite Structures, 1989;13:251-274.

[15] Czyz, J. A., Szyszkowski, W. An Effective Method for Non-Linear Viscoelastic Structural Analysis. Computers & Structures, 1990;37(5): 637-646.

Figure Captions

Figure 1: Laminated composite cylinder (after [2]).

Figure 2: Time-dependent axial stress in the viscoelastic material.

Figure 3: Hoop stress in the viscoelastic material after 10^6 min.

Figure 4: Radial stress in the viscoelastic material after 10^6 min.

Figure 5: Scheme of load distribution in a thin cylinder under internal pressure.

Figure 6: Scheme of load distribution in a thin cylinder under external pressure.

Figure 7: Scheme of load distribution in a thin cylinder under axial loading.

Figure 8: External axial and hoop strain time-dependent evolution for cylinders [45/-45/-45/45] under internal pressure with inner radius to thickness ratios R_i /h of 100, 10, 5 and 2.

Figure 9: External axial and hoop strain time-dependent evolution for cylinders [54/-54/-54/54] under internal pressure with inner radius to thickness ratios R_i /h of 100, 10, 5 and 2.

Figure 10: Axial and hoop stress distribution immediately after loading (t=0) for cylinders [54/-54/-54/54] under internal pressure with inner radius to thickness ratios R_i /h of 100, 10, 5 and 2.

Figure 11: Axial and hoop stress distribution the instant t=10^5 min for cylinders [54/-54/-54/54] under internal pressure with inner radius to thickness ratios R_i /h of 100, 10, 5 and 2.

Figure 12: External axial and hoop strain time-dependent evolution for cylinders [54/-54/-54/54] under external pressure with inner radius to thickness ratios R_i /h of 100, 10, 5 and 2.

Figure 13: Axial and hoop stress distribution immediately after loading (t=0) for cylinders [54/-54/-54/54] under external pressure with inner radius to thickness ratios R_i /h of 100, 10, 5 and 2.

Figure 14: Axial and hoop stress distribution at the instant t=10^5 min for cylinders [54/-54/-54/54] under external pressure with inner radius to thickness ratios R_i /h of 100, 10, 5 and 2.

Figure 15: External axial and hoop strain time-dependent evolution for cylinders [54/-54/-54/54] under axial compressive load with inner radius to thickness ratios R_i /h of 100, 10, 5 and 2.

Figure 16: Axial and hoop stress distribution immediately after loading (t=0) for cylinders [54/-54/-54/54] under axial compressive load with inner radius to thickness ratios R_i /h of 100, 10, 5 and 2.

Figure 17: Axial and hoop stress distribution at the instant t=10^5 min for cylinders [54/-54/-54/54] under axial compressive load with inner radius to thickness ratios R_i /h of 100, 10, 5 and 2.

Figure 18: Radial stress distribution immediately after loading (t=0) for cylinders [54/-54/-54/54] under axial compressive load with inner radius to thickness ratios R_i /h of 100, 10, 5 and 2.

Figure 19: Radial stress distribution at the instant t=10^5 min for cylinders [54/-54/-54/54] under axial compressive load with inner radius to thickness ratios R_i /h of 100, 10, 5 and 2.

Figure 20: Shear stress distribution immediately after loading (t=0) for cylinders [54/-54/-54/54] under axial compressive load with inner radius to thickness ratios R_i /h of 100, 10, 5 and 2.

Figure 21: Shear stress distribution at the instant t=10^5 min for cylinders [54/-54/-54/54] under axial compressive load with inner radius to thickness ratios R_i /h of 100, 10, 5 and 2.

List of Tables

Table I. Shear relaxation modulus data (equation 26).

i	G_i MPa	τ_i min
0	462	
1	32	1
2	72	10
3	165	95
4	590	822
5	748	7224
6	703	65632
7	690	370698

Table II. Shear creep compliance used in RESFLU.

i	S_i	λ_i
0	2.89E-01	
1	1.42E+00	1.00E-06
2	2.31E-01	1.00E-05
3	1.38E-01	1.00E-04
4	6.49E-02	1.00E-03
5	1.46E-02	1.00E-02
6	6.20E-03	1.00E-01
7	2.71E-03	1.00E+00

Table III. Elastic properties of T300/5208

E_1 GPa	E_2 GPa	G_{12} GPa	ν_{12}	ν_{23}
132	9.434	6.41	0.273	0.273

Table IV. Transverse and shear creep compliance of T300/5208

i	$S_{22,i}$ GPa^{-1}	$\lambda_{22,i}$ min^{-1}	$S_{66,i}$ GPa^{-1}	$\lambda_{66,i}$ min^{-1}
0	0.10600		0.15601	
1	0.00104	1	0.00235	1
2	0.00119	10^{-1}	0.00232	10^{-1}
3	0.00281	10^{-2}	0.00506	10^{-2}
4	0.00499	10^{-3}	0.00823	10^{-3}
5	0.01063	10^{-4}	0.01567	10^{-4}
6	0.01779	10^{-5}	0.02434	10^{-5}
7	0.05460	10^{-6}	0.06500	10^{-6}

Table V. Transverse and shear creep compliance of T300/5208

*Function**	*Coefficient*	
	α	β (MPa)
$g_{0,22}$	0.00000	
$g_{1,22}$	0.08750	6.43
$g_{2,22}$	0.00000	
$a_{\sigma,22}$	0.24700	6.43
$g_{0,66}$	0.00513	12.05
$g_{1,66}$	0.00979	7.23
$g_{2,66}$	0.12400	7.23
$a_{\sigma,66}$	0.03400	14.50

* $g_{i,jj} = 1.0 + \alpha\langle\tau_{oct} - \beta\rangle$, $a_{\sigma,jj} = \exp\left(-\alpha\langle\tau_{oct} - \beta\rangle\right)$

List of Figures

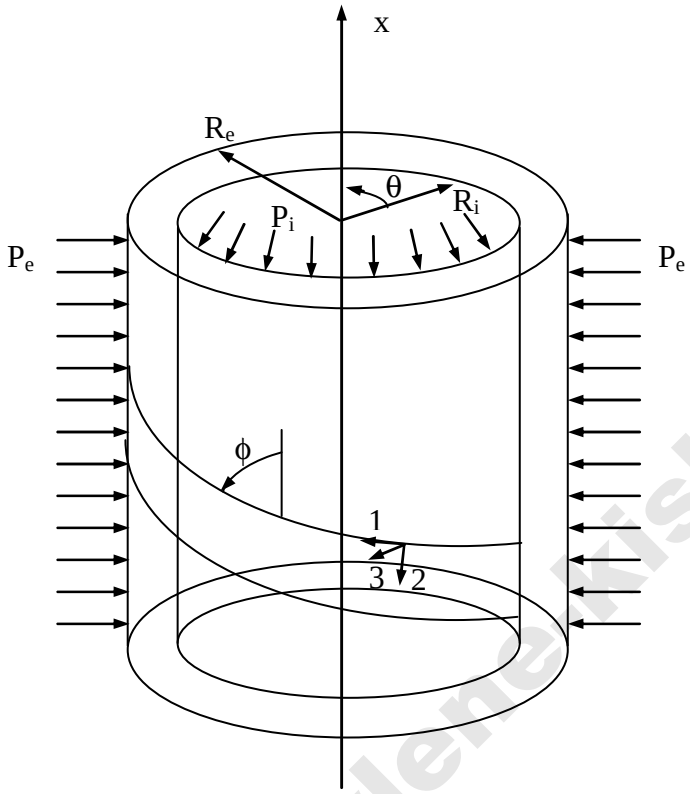

Figure 1: Laminated composite cylinder (after [2]).

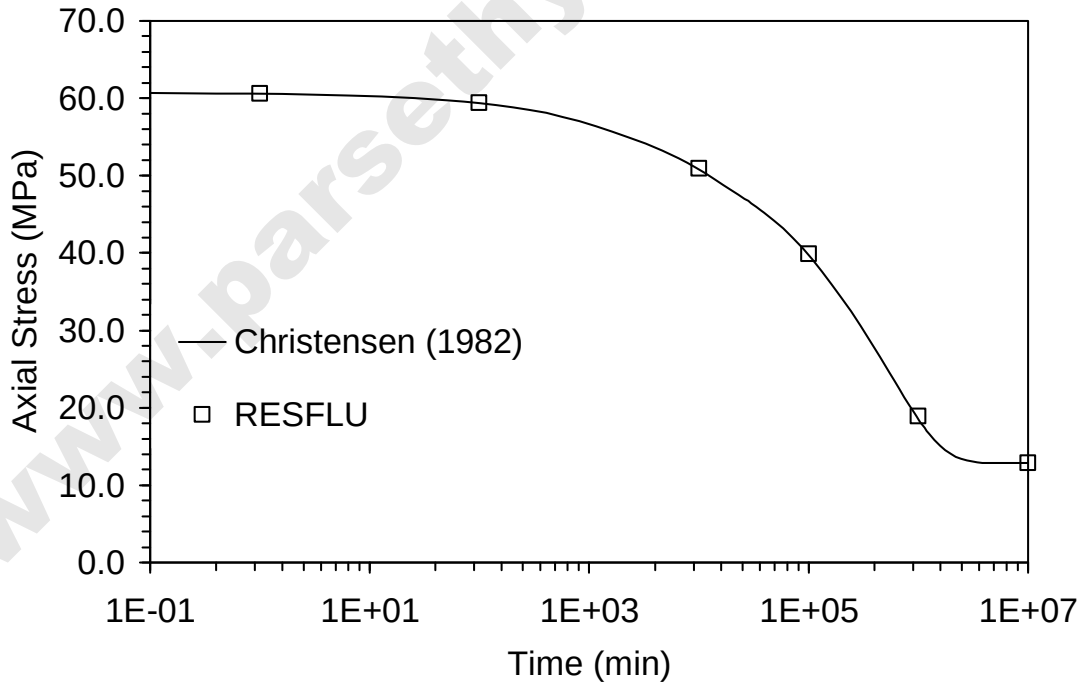

Figure 2: Time-dependent axial stress in the viscoelastic material.

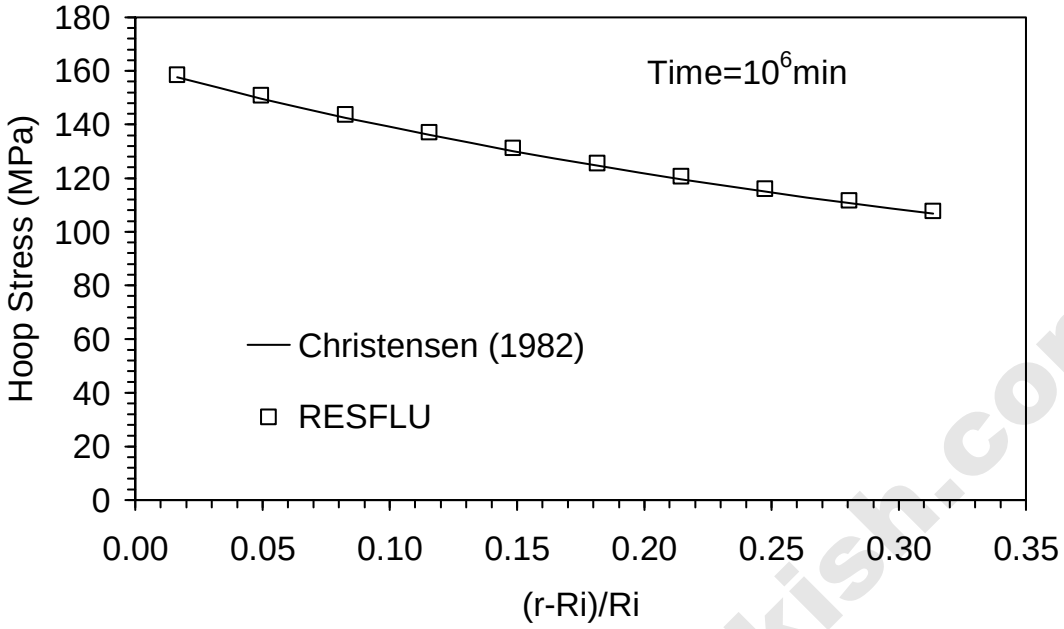

Figure 3: Hoop stress in the viscoelastic material after 10^6 min.

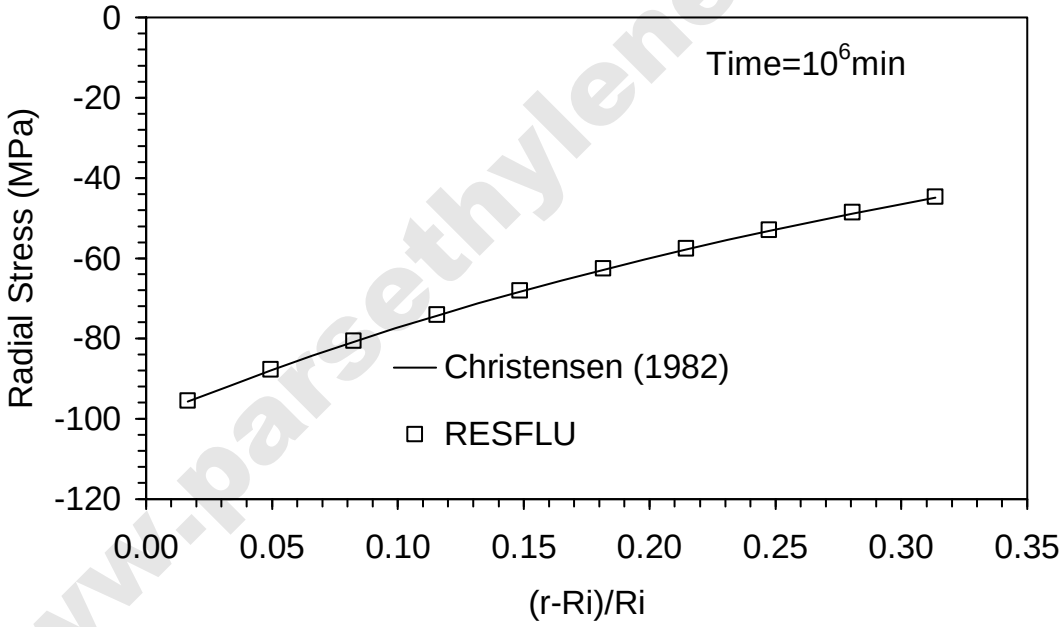

Figure 4: Radial stress in the viscoelastic material after 10^6 min.

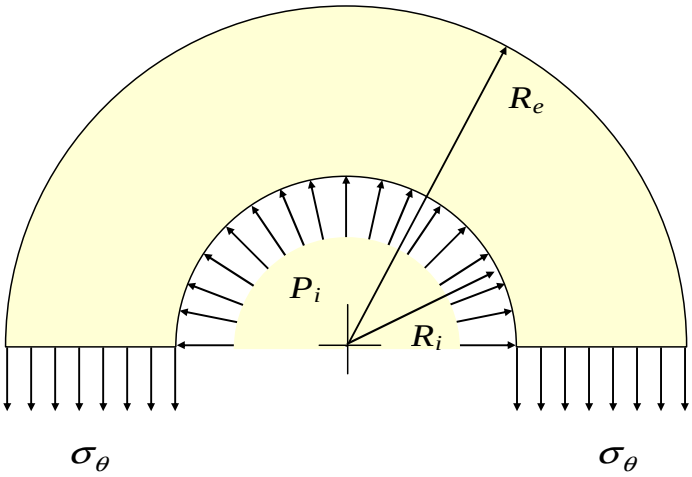

Figure 5: Scheme of load distribution in a thin cylinder under internal pressure.

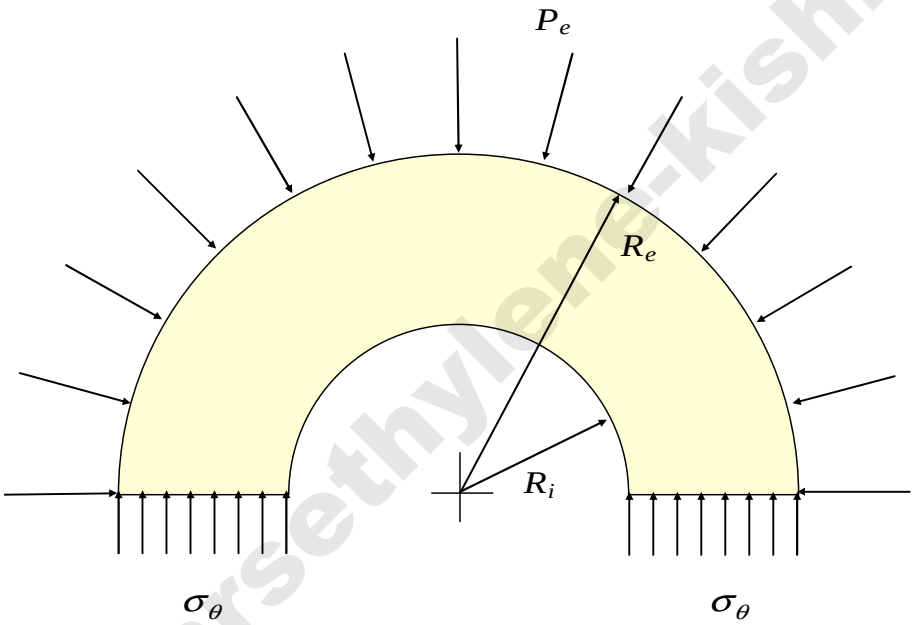

Figure 6: Scheme of load distribution in a thin cylinder under external pressure.

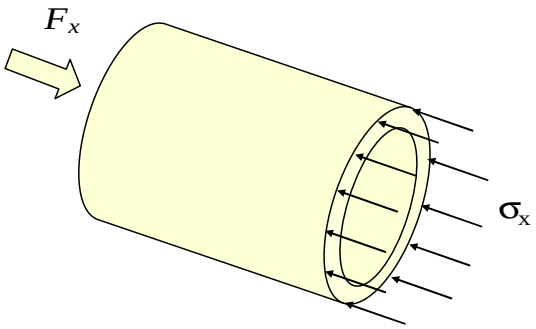

Figure 7: Scheme of load distribution in a thin cylinder under axial loading.

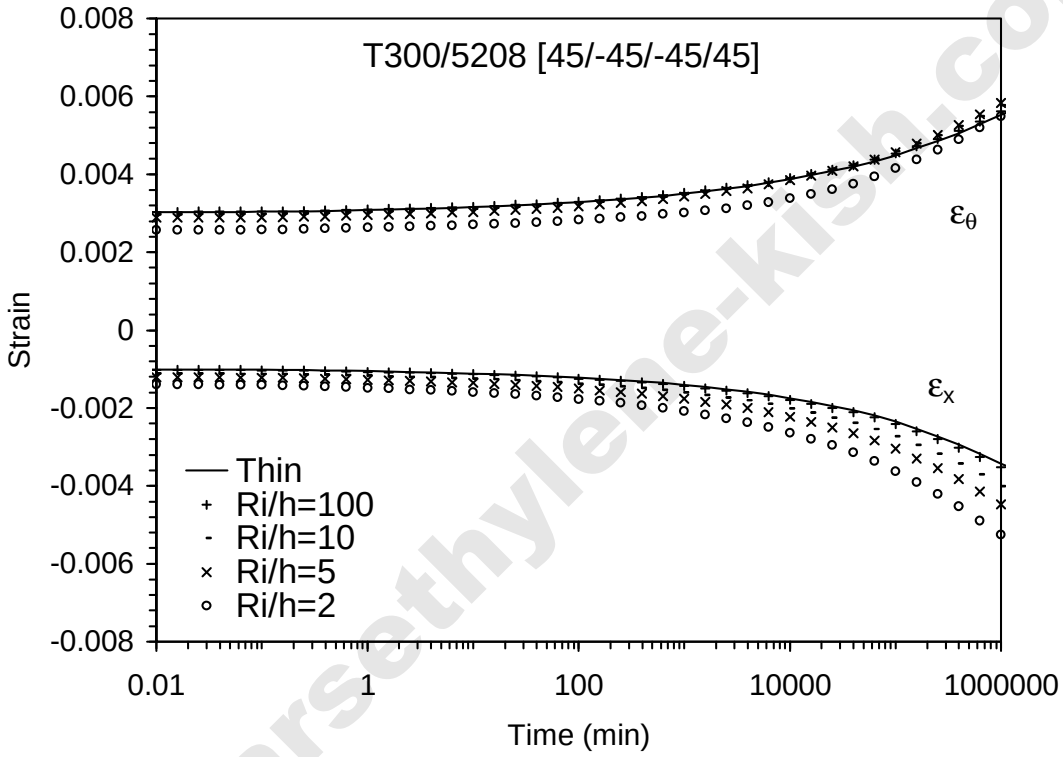

Figure 8: External axial and hoop strain time-dependent evolution for cylinders [45/-45/-45/45] under internal pressure with inner radius to thickness ratios R_i /h of 100, 10, 5 and 2.

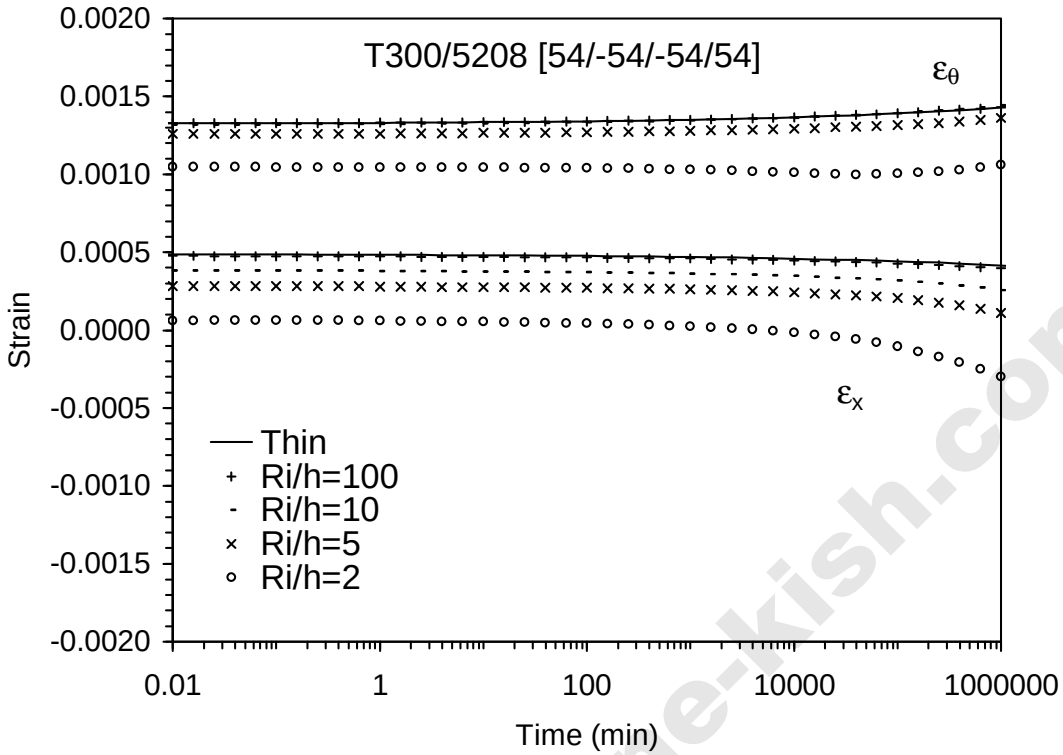

Figure 9: External axial and hoop strain time-dependent evolution for cylinders [54/-54/-54/54] under internal pressure with inner radius to thickness ratios R_i /h of 100, 10, 5 and 2.

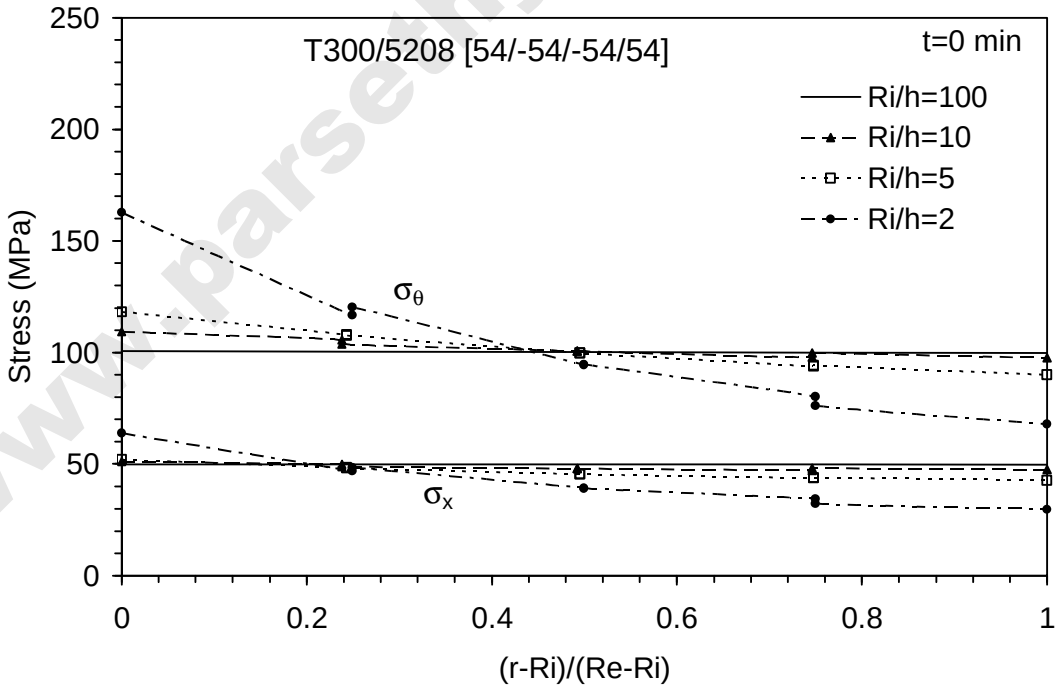

Figure 10: Axial and hoop stress distribution immediately after loading (t=0) for cylinders [54/-54/-54/54] under internal pressure with inner radius to thickness ratios R_i/h of 100, 10, 5 and 2.

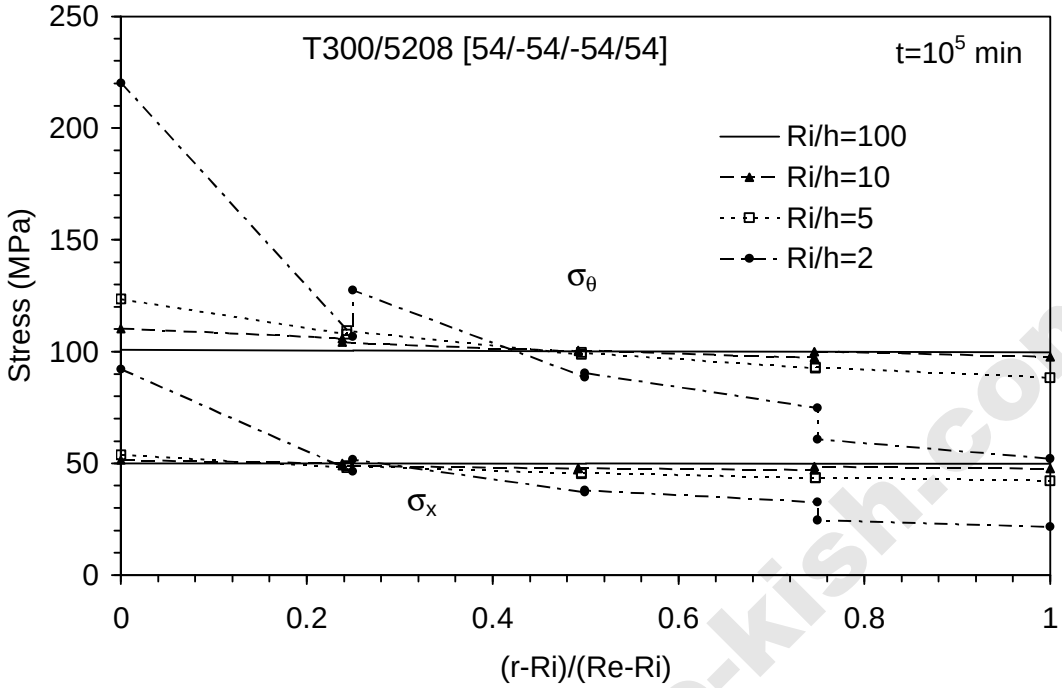

Figure 11: Axial and hoop stress distribution the instant t=10^5 min for cylinders [54/-54/-54/54] under internal pressure with inner radius to thickness ratios R_i /h of 100, 10, 5 and 2.

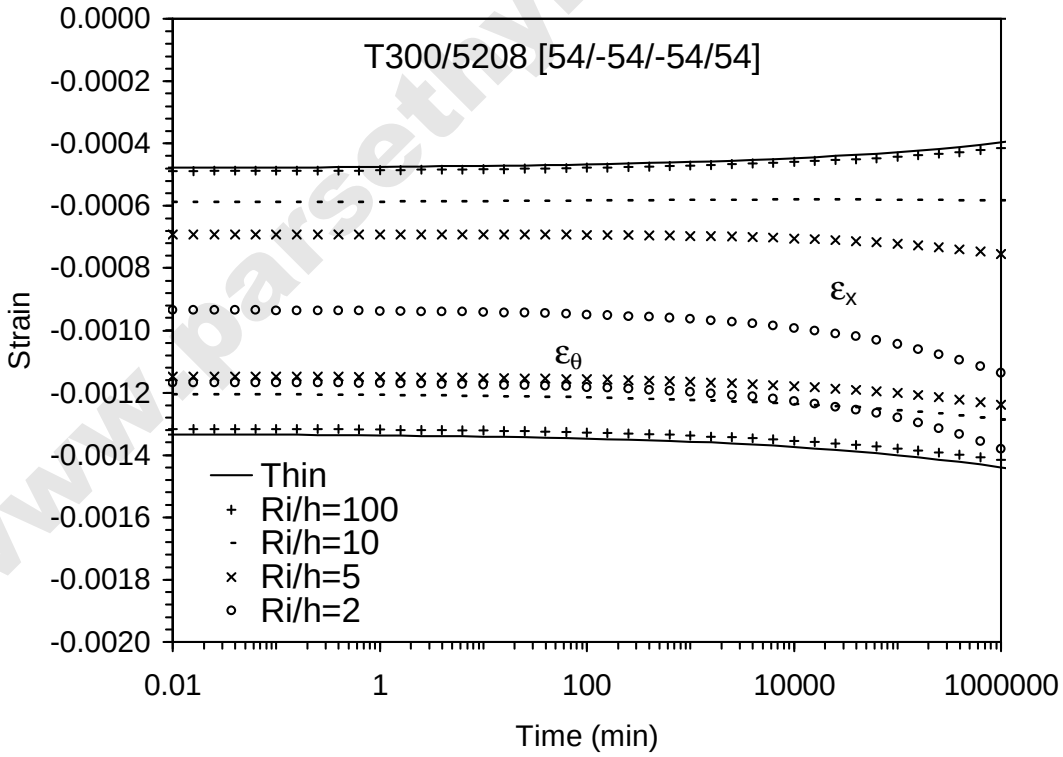

Figure 12: External axial and hoop strain time-dependent evolution for cylinders [54/-54/-54/54] under external pressure with inner radius to thickness ratios R_i /h of 100, 10, 5 and 2.

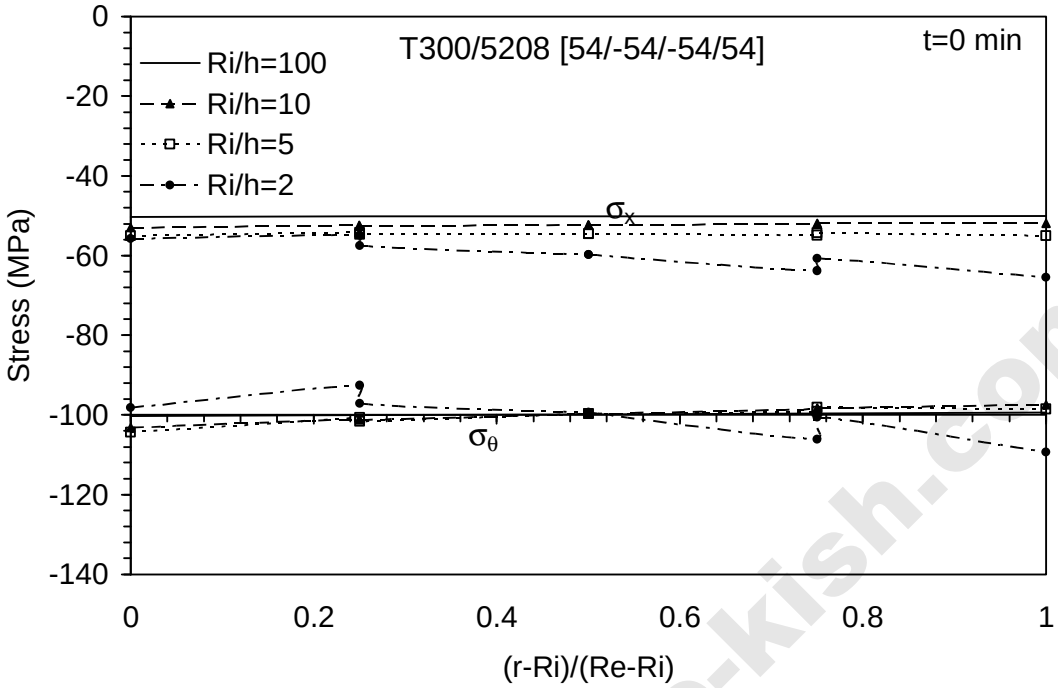

Figure 13: Axial and hoop stress distribution immediately after loading (t=0) for cylinders [54/-54/-54/54] under external pressure with inner radius to thickness ratios R_i/h of 100, 10, 5 and 2.

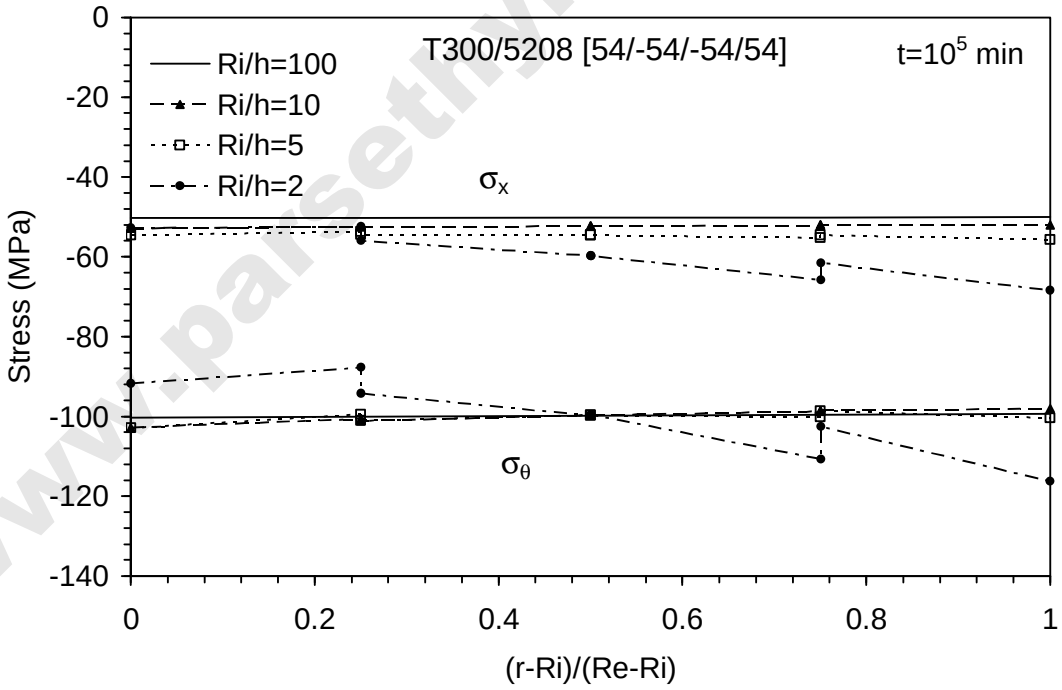

Figure 14: Axial and hoop stress distribution at the instant t=10^5 min for cylinders [54/-54/-54/54] under external pressure with inner radius to thickness ratios R_i/h of 100, 10, 5 and 2.

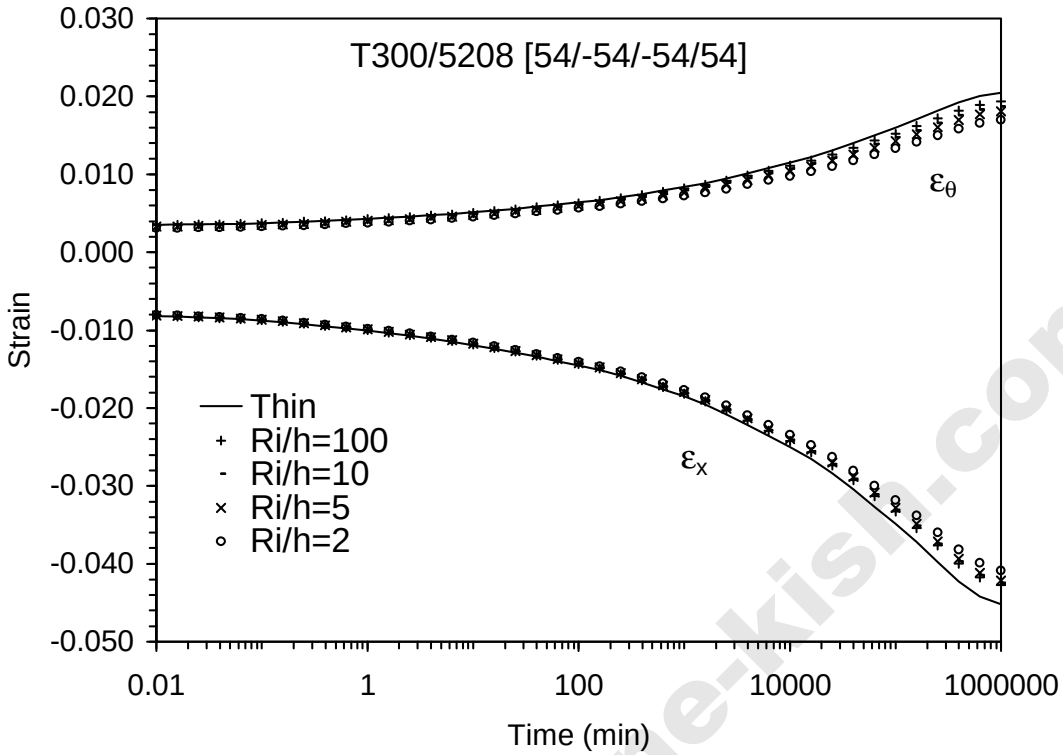

Figure 15: External axial and hoop strain time-dependent evolution for cylinders [54/-54/-54/54] under axial compressive load with inner radius to thickness ratios R_i /h of 100, 10, 5 and 2.

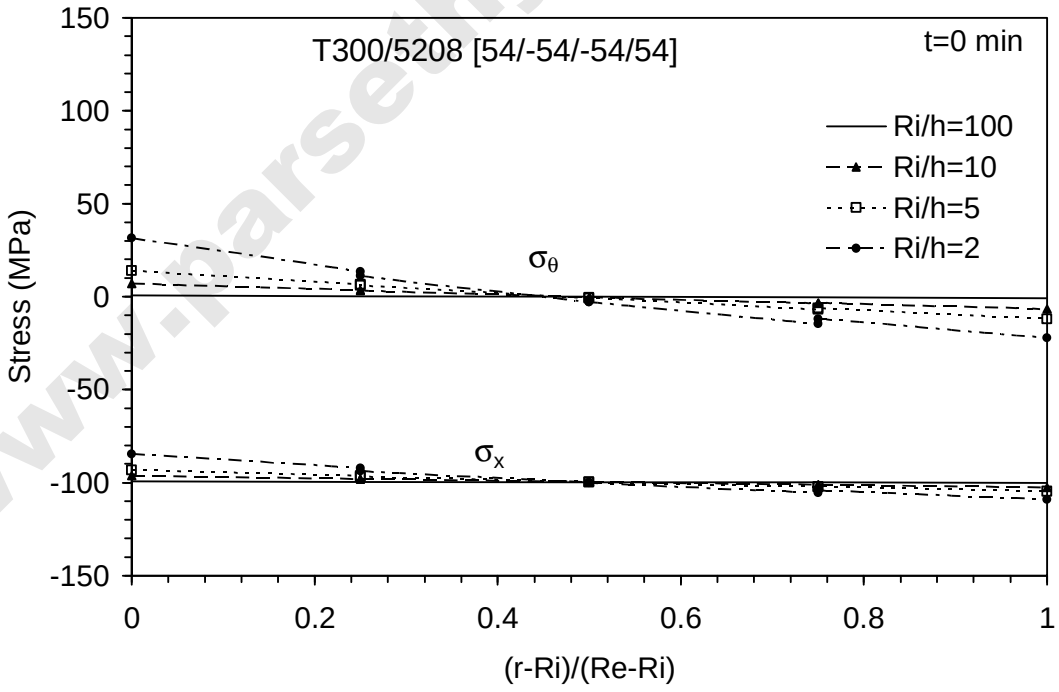

Figure 16: Axial and hoop stress distribution immediately after loading (t=0) for cylinders [54/-54/-54/54] under axial compressive load with inner radius to thickness ratios R_i /h of 100, 10, 5 and 2.

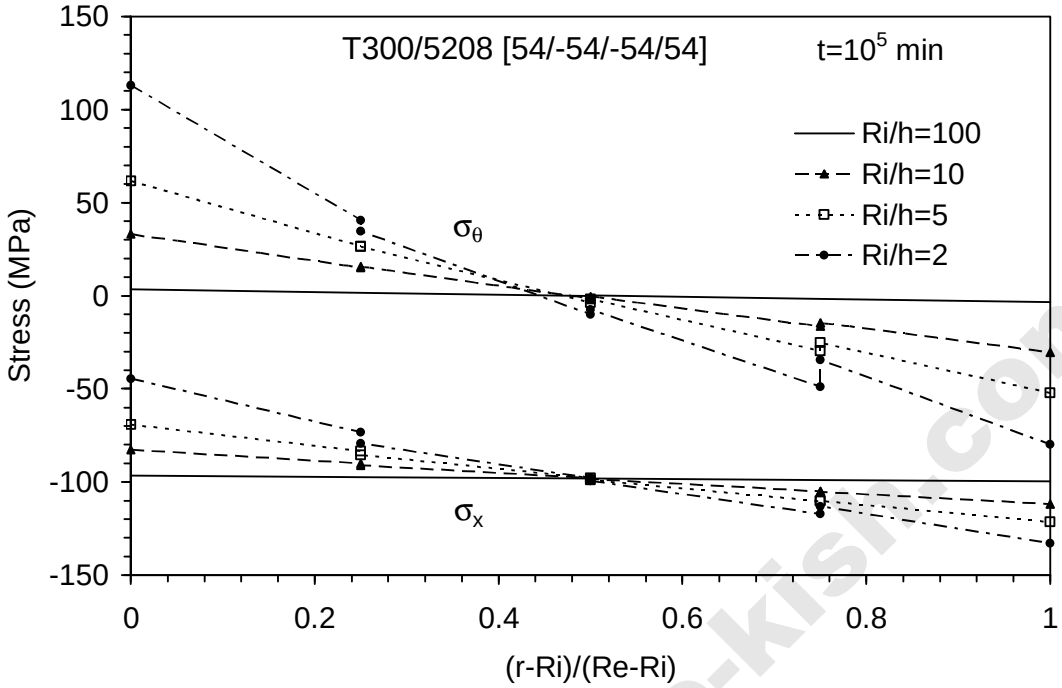

Figure 17: Axial and hoop stress distribution at the instant t=10^5 min for cylinders [54/-54/-54/54] under axial compressive load with inner radius to thickness ratios R_i /h of 100, 10, 5 and 2.

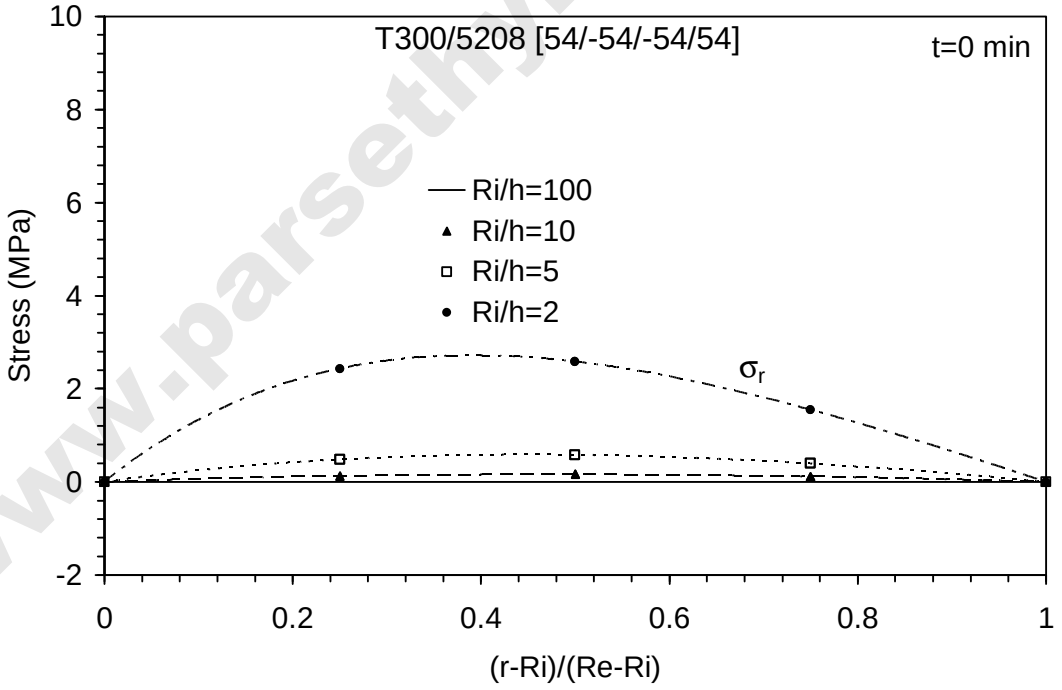

Figure 18: Radial stress distribution immediately after loading (t=0) for cylinders [54/-54/-54/54] under axial compressive load with inner radius to thickness ratios R_i /h of 100, 10, 5 and 2.

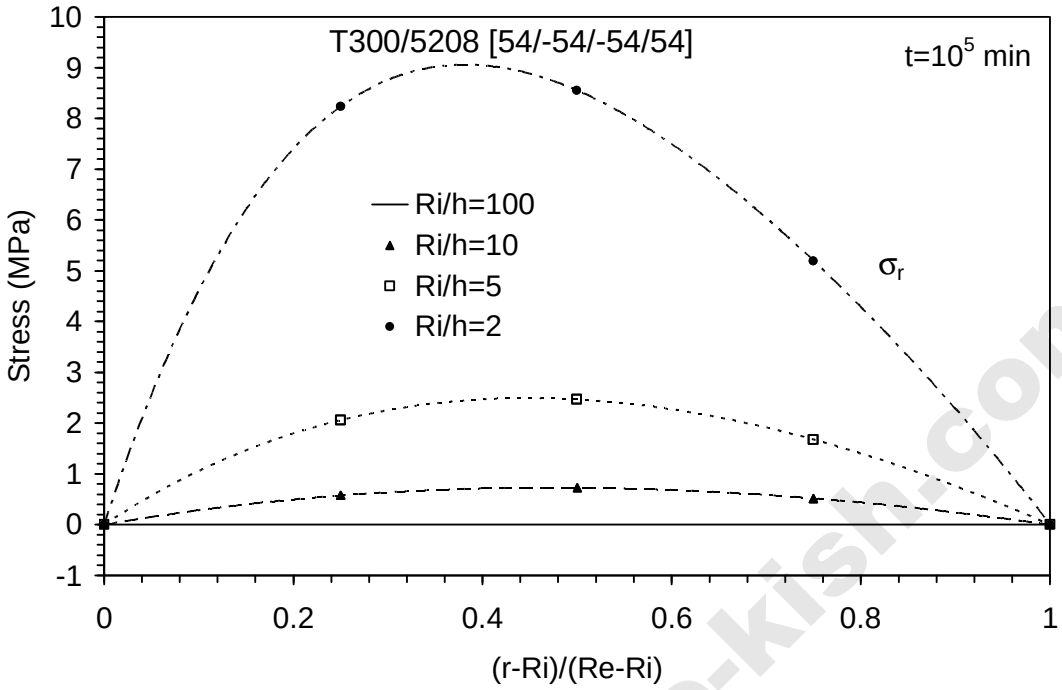

Figure 19: Radial stress distribution at the instant $t=10^5$ min for cylinders [54/-54/-54/54] under axial compressive load with inner radius to thickness ratios R_i /h of 100, 10, 5 and 2.

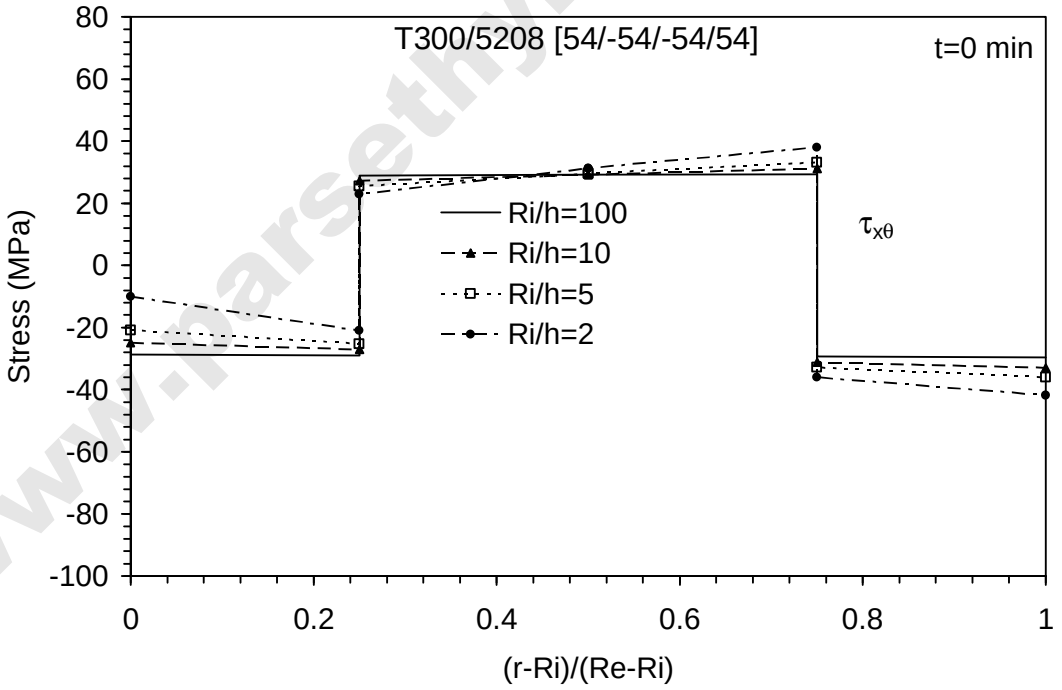

Figure 20: Shear stress distribution immediately after loading (t=0) for cylinders [54/-54/-54/54] under axial compressive load with inner radius to thickness ratios R_i /h of 100, 10, 5 and 2.

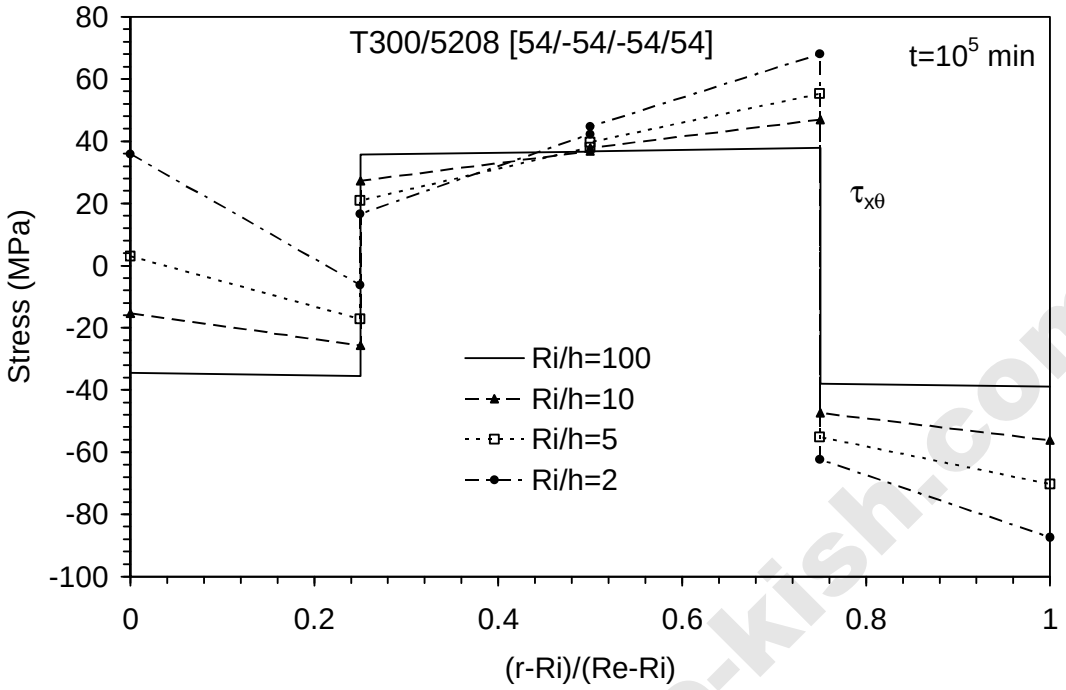

Figure 21: Shear stress distribution at the instant $t=10^5$ min for cylinders [54/-54/-54/54] under axial compressive load with inner radius to thickness ratios R_i/h of 100, 10, 5 and 2.